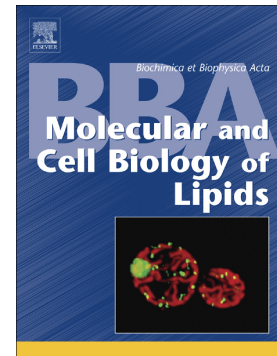


Accepted Manuscript

Poly(ADP-ribose) polymerase-2 is a lipid-modulated modulator of muscular lipid homeostasis

Judit Márton, Mária Péter, Gábor Balogh, Beáta Bódi, Andras Vida, Magdolna Szántó, Dora Bojcsuk, Laura Jankó, Harjit Pal Bhattoa, Imre Gombos, Karen Uray, Ibolya Horváth, Zsolt Török, Balint L. Balint, Zoltán Papp, László Vígh, Péter Bai



PII: S1388-1981(18)30187-2
DOI: doi:[10.1016/j.bbalip.2018.07.013](https://doi.org/10.1016/j.bbalip.2018.07.013)
Reference: BBAMCB 58338
To appear in: *BBA - Molecular and Cell Biology of Lipids*
Received date: 22 January 2018
Revised date: 22 July 2018
Accepted date: 29 July 2018

Please cite this article as: Judit Márton, Mária Péter, Gábor Balogh, Beáta Bódi, Andras Vida, Magdolna Szántó, Dora Bojcsuk, Laura Jankó, Harjit Pal Bhattoa, Imre Gombos, Karen Uray, Ibolya Horváth, Zsolt Török, Balint L. Balint, Zoltán Papp, László Vígh, Péter Bai , Poly(ADP-ribose) polymerase-2 is a lipid-modulated modulator of muscular lipid homeostasis. *Bbamcb* (2018), doi:[10.1016/j.bbalip.2018.07.013](https://doi.org/10.1016/j.bbalip.2018.07.013)

This is a PDF file of an unedited manuscript that has been accepted for publication. As a service to our customers we are providing this early version of the manuscript. The manuscript will undergo copyediting, typesetting, and review of the resulting proof before it is published in its final form. Please note that during the production process errors may be discovered which could affect the content, and all legal disclaimers that apply to the journal pertain.

Poly(ADP-ribose) polymerase-2 is a lipid-modulated modulator of muscular lipid homeostasis

Judit Márton¹, Mária Péter², Gábor Balogh², Beáta Bódi³, Andras Vida^{1,4}, Magdolna Szántó¹, Dora Bojcsuk⁵, Laura Jankó¹, Harjit Pal Bhattoa⁶, Imre Gombos², Karen Uray¹, Ibolya Horváth², Zsolt Török², Balint L Balint⁵, Zoltán Papp^{3,7}, László Vígh², Péter Bai^{1,4,8,*}

¹Department of Medical Chemistry, Faculty of Medicine, University of Debrecen, 4032, Hungary

²Biological Research Center of the Hungarian Academy of Sciences, Szeged, 6726, Hungary

³Division of Clinical Physiology, Faculty of Medicine, University of Debrecen, 4032, Hungary

⁴MTA-DE Lendület Laboratory of Cellular Metabolism Research Group, Debrecen, 4032, Hungary

⁵Department of Biochemistry and Molecular Biology, Faculty of Medicine, University of Debrecen, 4032, Hungary

⁶Department of Laboratory Medicine, Faculty of Medicine, University of Debrecen, 4032, Hungary

⁷HAS-UD Vascular Biology and Myocardial Pathophysiology Research Group, Hungarian Academy of Sciences, Debrecen 4012, Hungary

⁸Research Center for Molecular Medicine, Faculty of Medicine, University of Debrecen, 4032, Hungary

Running title: PARP2 modulates lipid metabolism

*All correspondence regarding this article should be sent to this author at the Department of Medical Chemistry, Faculty of Medicine, University of Debrecen, H- 4032 Debrecen, Egyetem tér 1, Hungary; Tel: +36 52 412 345; Fax: +36 52 412 566; E-mail: bai@med.unideb.hu

Abstract

There is a growing body of evidence that poly(ADP-ribose) polymerase-2 (PARP2), although originally described as a DNA repair protein, has a widespread role as a metabolic regulator. We show that the ablation of PARP2 induced characteristic changes in the lipidome. The silencing of PARP2 induced the expression of sterol regulatory element-binding protein-1 and -2 and initiated *de novo* cholesterol biosynthesis in skeletal muscle. Increased muscular cholesterol was shunted to muscular biosynthesis of dihydrotestosterone, an anabolic steroid. Thus, skeletal muscle fibers in PARP2^{-/-} mice were stronger compared to those of their wild-type littermates. In addition, we detected changes in the dynamics of the cell membrane, suggesting that lipidome changes also affect the biophysical characteristics of the cell membrane. In *in silico* and wet chemistry studies, we identified lipid species that can decrease the expression of PARP2 and potentially phenocopy the genetic abruption of PARP2, including artificial steroids. In view of these observations, we propose a new role for PARP2 as a lipid-modulated regulator of lipid metabolism.

Keywords

androgen/cholesterol/PARP/skeletal muscle/dihydrotestosterone

Introduction

Poly(ADP-ribose) polymerase-2 (PARP2, ARTD2) is a member of the PARP family [1, 2]. PARP2 binds to DNA strand breaks or RNA species [3-6] where it is activated. Active PARP2 cleaves nicotinamide-adenine dinucleotide (NAD⁺) to nicotinamide and ADP-ribose, and forms poly(ADP-ribose) polymers (PAR) on acceptor proteins [7]. PARylation often changes the biochemical properties of proteins [8, 9]. PARP2 is responsible for 10-15% of total cellular PARP activity; the remaining activity is mostly due to PARP1 [10, 11].

Although PARP2 was originally described as a DNA repair/maintenance enzyme [10, 12], recent studies have widened the scope of its biological roles [8, 9]. Importantly, PARP2 modulates transcription [13, 14] through interactions with numerous transcription factors (PPARs, TTF1, ER α , LXRs, FXRs) [15-17]. Changes in transcription are major drivers behind PARP2-mediated phenotypes [11, 14, 16, 18-24].

PARP2 was shown to be involved in metabolic regulation, including lipid metabolism (reviewed in [25, 26]). The observation that PARP2 was a positive cofactor of PPAR γ and facilitated fat accumulation in white adipose tissue (WAT) [15] demonstrated the role of PARP2 in lipid metabolism for the first time. The deletion of PARP2 disrupts lipid deposition in WAT [15]. However, in PARP2 knockout mice, no atopic lipid is deposited in the liver or skeletal muscle [18], probably due to increased lipid oxidation, which is detectable at the organismal level as decreased respiratory quotient [18]. Increased lipid oxidation stems from the induction of sirtuin-1 (SIRT1) expression and activity, resulting in mitochondrial biogenesis in the skeletal muscle and liver [18, 21].

PARP2 also impacts another arch of lipid metabolism through cholesterol biosynthesis and lipoprotein metabolism. PARP2 is a repressor of sterol regulatory element binding protein-1 (SREBP1) expression [14]. In the absence of PARP2, SREBP1 expression and activation increase in the liver, culminating in increased hepatic cholesterol content [14]. Interestingly, while the enterohepatic circulation of cholesterol does not change in PARP2^{-/-} mice, the systemic circulation of cholesterol is impaired, marked by lower high-density lipoprotein levels through decreases in hepatic ATP-binding cassette sub-family A Member 1 (ABCA1) expression [14].

In addition to having these functions, PARP2 had been associated with lipid metabolism in a genome-wide association study [27], suggesting that there might be other physiologically relevant PARP2-mediated changes in lipid metabolism. Skeletal muscle is a major energy expender in humans and is strongly affected by changes in PARP2 expression [18], which prompted us to perform a wide-scale assessment of PARP2-mediated changes in skeletal muscle lipid metabolism.

Results

The silencing or deletion of PARP2 leads to characteristic changes in the lipidome

As a first step, we validated our models by assessing PARP2 expression in PARP2 knockout mice [28] and in C2C12 cells in which PARP2 was silenced by lentiviral transduction of an shRNA construct [18] (**Fig. 1A, Fig. S1**). We performed a mass spectrometry-based lipidomic screening to detect the lipids involved in cell membrane synthesis in the skeletal muscle of PARP2^{+/+} and PARP2^{-/-} mice, as well as in scPARP2 and shPARP2 transfected cells. When we subjected the results to orthogonal partial least squares discrimination analysis (OPLS-DA), both scPARP2 and shPARP2 C2C12 cells and skeletal muscle samples from PARP2^{+/+} and PARP2^{-/-} mice were clearly separated (**Fig. 1B**). Validation of the model was performed by permutation tests (n = 1000), which returned good predictability: Q2 = 0.84 (p = 0.05) for cells and Q2 = 0.57 (p = 0.002) for skeletal muscles. These data suggest deep and characteristic changes in the lipidome due to inhibition of PARP2.

The silencing of PARP2 leads to higher muscular cholesterol and anabolic steroid content

As a next step, we compared the steady-state gene expression profile of C2C12 cells transfected with scPARP2 or shPARP2 to provide an explanation for the changes in Figure 1. The analysis revealed the dysregulation of 756 genes, of which 429 were downregulated and 327 were upregulated. Gene ontology analysis of the hits revealed the dysregulation of genes involved in muscular function and metabolism (**Fig. 2A, Table 1**). Among these genes, we identified increases in the expression of *Tnn1*, *Tnnc*, and *Tnnt3*, which are markers of oxidative, type I, slow-twitch fibers in shPARP2 cells. As the deletion of PARP2 is linked to increased proportions of type I fibers [18], increased expression of *Tnn1*, *Tnnc*, and *Tnnt3* validates our findings. Among the metabolic genes, we identified several [29] lipid metabolism-related genes, of which 22 were upregulated (**Fig. 2A, Table 1**).

A thorough analysis of the lipid metabolism genes revealed that *Srebp1*, *Srebp2*, and several of their downstream targets (*Cyp7a1*, *Fdps*, *Ldlr*, *Acly*, *Hmgcr*, *Acaca*, and *Scd2*) were upregulated at the mRNA level in C2C12 cells transfected with shPARP2 compared to scPARP2-transfected cells. These same lipid metabolism genes were upregulated in the skeletal muscle of PARP2^{-/-} compared to PARP2^{+/+} male mice (**Fig. 2B**). Increases in the expression of SREBP1 and SREBP2 were dependent on the induction of their promoters, as suggested by luciferase reporter assays (**Fig. 2C**).

We assessed whether changes in the expression of SREBP target genes after silencing of PARP2 are indeed related to changes in SREBP expression. To that end, SREBP1 and

SREBP2 were silenced in scPARP2 and shPARP2 C2C12 cells (**Fig. 2D, Fig. S2**). Silencing of SREBP1 and SREBP2 abolished the increased expression of HMGCR (**Fig. 2E**), pointing toward the involvement of both SREBPs in the PARP2-elicited effects.

SREBP1 and SREBP2 are lipid biosynthetic transcription factors that reside in the endoplasmic reticulum and Golgi, bound to scaffold proteins, when in the presence of sterols [29]. When cholesterol concentrations decrease, SREBPs undergo proteolytic processing and translocate to the nucleus, where they bind to promoters and induce a specific gene set, leading to cholesterol biosynthesis and accumulation [29]. We have observed that increases in SREBP1 and SREBP2 mRNA levels and their downstream target, HMGCR, result in increases in the corresponding proteins in PARP2 knockdown cells and in the gastrocnemius muscle of PARP2^{-/-} mice (**Fig. 3A, Fig. S3A**). Moreover, in cells, the nuclear processed forms of SREBP1 and SREBP2 were also increased upon PARP2 silencing (**Fig. 3A, Fig. S3A**), as demonstrated by immunocytochemistry studies showing enhanced accumulation of SREBP1 and SREBP2 in the nucleus (**Fig. 3B**).

The question arose whether proteolytic processing of SREBP1 and SREBP2 would be affected by the silencing of PARP2. The expression of the proteins involved in SREBP maturation (*Insig1a*, *Scap*, *Sp1*, *Sp2*) was unaltered between scPARP2 and shPARP2 C2C12 cells (**Fig. 3C**). Similarly, treatment of cells with an inhibitor of the proteolytic processing of SREBPs, betulin [30], reverted SREBP processing both in scPARP2 and shPARP2 C2C12 cells (**Fig. 3D, Fig. S3B**), suggesting that SREBP processing is unaltered when PARP2 is silenced. The enhanced activation of SREBP1 and -2 culminated in increased total cholesterol content in both C2C12 cells transfected with shPARP2 and skeletal muscle of PARP2^{-/-} male mice (**Fig. 3E**).

We next wanted to assess whether muscular cholesterol causes muscular steroidogenesis. We measured the expression of steroidogenic enzymes involved in the conversion of cholesterol to testosterone (anabolic steroids). Out of the genes we assessed, *Star*, *Hsd17b11*, *Srd5a1*, and *Srd5a2* were induced in cells or tissues depleted of PARP2 (**Fig. 4A**). Increases in the expression of *Star* and *Srd5a1* were dependent on the activation of the promoters of these genes as highlighted by luciferase reporter assays (**Fig. 4B**). *Star*, the commitment enzyme toward steroidogenesis, and 5- α -reductase isoforms, which are at the “output end” of steroidogenesis, were induced in the absence of PARP2. Changes in the expression of the steroidogenic machinery were translated into changes in muscular steroids. Dihydrotestosterone (DHT) levels were higher, whereas androstenedione did not change and testosterone levels were lower in the muscles of the PARP2^{-/-} mice (**Fig 4C**). Importantly, these changes were restricted to the muscle, as the expression of key PARP2-mediated steroidogenic enzymes remained unchanged in the suprarenal gland and testis of PARP2^{-/-} mice compared to those of PARP2^{+/+} mice (**Fig. S4A**). Serum DHT levels showed a

minor decrease (**Fig. S4B**). Increases in the expression of SREBP-dependent genes and anabolic steroids were absent in PARP2^{-/-} female mice (**Fig. S4C**).

Deletion of PARP2 augmented skeletal muscle contractile function

Testosterones, especially DHT, have an anabolic effect on skeletal muscle [31], which prompted us to assess muscle strength. Force production was monitored under isometric conditions in single slow and fast twitch skeletal muscle fibers isolated from two mixed-type muscles, the gastrocnemius muscle and the diaphragm, of PARP2^{+/+} and PARP2^{-/-} male mice. Ca²⁺-independent passive force (F_{passive}) was not statistically different in skeletal myofibers from PARP2^{+/+} and PARP2^{-/-} mice (**Fig. 5A**). Ca²⁺-dependent active force (F_{active}) at submaximal levels of activation and Ca²⁺-activated maximal force production (F_{max} , pCa 4.75) were higher in both muscles of PARP2^{-/-} males compared to those of PARP2^{+/+} animals, for both fast- and slow-twitch fibers (**Fig. 5B**). For the characterization of Ca²⁺ sensitivity of isometric force production, F_{active} was normalized to F_{max} for each skeletal muscle fiber (pCa₅₀). The pCa₅₀ values were significantly higher in fast-twitch fibers of gastrocnemius and diaphragm muscles in PARP2^{-/-} mice compared to those of PARP2^{+/+} mice. (**Fig. 5C**). Taken together, the data show that the loss of PARP2 augmented active force production irrespective of muscle fiber type.

Silencing of PARP2 changes lateral diffusion of BODIPY FL-SM

Complex changes in the lipidome may lead to changes in cell membrane structure. To monitor dynamic changes in the plasma membranes, we assessed the lateral diffusion and confinement properties of a fluorescent probe, BODIPY FL-SM (a sphingomyelin-derivative probe). The diffusion coefficient (D) and confinement time (τ_0) describe the lateral diffusion of the probe and the organization of the membrane, respectively, and can be calculated from the diffusion law graph [32]. We observed increases in the D and in the τ_0 for the probe (**Fig. 6A-B**), indicating that both the speed and the confinement of the diffusion of the probe were higher in the membranes of PARP2-silenced cells. This strongly suggests that the membrane dynamics of these cells significantly differ from those of the wild type.

Lipids can modulate the expression of PARP2

The results described above point to a possible role for PARP2 in the regulation of lipid homeostasis. Low PARP2 expression or the loss of PARP2 induced a phenotype characterized by lipidome changes and improved muscular contractile function. A recent study showed that α -lipoic acid downregulates PARP2 expression [33], suggesting that lipid-mediated regulatory circles may include changes in PARP2 expression. Lipids frequently exert their expression effects through nuclear receptors; therefore, we assessed the existing

data on nuclear receptor binding sites to identify transcription factors that could be responsible for the binding of these lipid species. We performed a screening for nuclear receptors that can serve as lipid sensors and translate changes in the lipid environment into gene expression programs. We identified a wide variety of nuclear receptor binding elements (half sites or inverted and direct repeats separated by different base pairs-long spacers) on the *PARP2* gene and in its vicinity. Therefore, we selected publicly available ChIP-seq (chromatin immunoprecipitation followed by deep sequencing) data derived from different organisms and cell lines to identify which nuclear receptor(s) bind(s) within the examined region. We found that upon calcitriol (1,25-(OH)₂D₃) treatment, the vitamin D receptor (VDR) binds to the promoter region of the *Parp2* gene in mice and also in the gene body between exons 4 and 5. The VDR binding site on the promoter region overlaps with the non-coding RNA *Rpph1* (also known as H1 RNA), and the summit position of this peak is located ~250 base pairs upstream of the transcription start site of *Parp2* (**Fig. 7A**). We next treated C2C12 cells with vitamin D, which increased the mRNA expression of *Parp2* and the VDR (**Fig. 8A**), suggesting that the VDR could indeed be the receptor that can physiologically regulate the expression of PARP2. Nevertheless, it should be stressed that other, yet unrevealed receptors or transcription factors may contribute to the lipid-mediated regulation of PARP2 mRNA expression.

We searched the NCBI GEO database for other lipids that potentially modulate the expression of PARP2. In addition to α -lipoic acid, we identified steroids, such as dexamethasone [34], medroxyprogesterone acetate, tibolone [35], and oxandrolone [36], that can downregulate PARP2 expression and potentially induce changes in lipid homeostasis. To validate these findings in cell experiments, we treated C2C12 cells with a large set of cholesterol derivatives (**Table 2**) and subsequently assessed the expression of PARP2. Out of the compounds used in the experiments, MPA, tibolone, LCA, and DCA were capable of downregulating the expression of PARP2 (**Fig. 8B**).

Discussion

In this study, we provide evidence that decreased PARP2 expression leads to widespread changes in lipid metabolism. This is achieved through enhancing SREBP1 and 2 transcription. SREBPs are central to the control of a variety of lipid biosynthetic pathways, including lipid desaturation and phospholipid and sterol biosynthesis [37]. PARP2 may induce adaptive responses to dietary/environmental stresses resulting in the maintenance of optimal membrane lipid composition, and profoundly affecting the biophysical properties of biological membranes.

We demonstrate that changes in lipid metabolism involve alterations in cell membrane lipid composition and synthesis of cholesterol and DHT that, altogether, strengthen muscular output. In addition, we show that some lipids can reduce PARP2 expression and, hence, produce changes in lipid metabolism similarly to the genetic deletion of PARP2.

SREBP1-dependent increases in cholesterol content upon decreased PARP2 expression have already been shown in the liver. Inhibition of PARP2 expression results in beneficial changes to the lipoprotein profile and decreased ABCA1 expression in the liver [14]. The current study provides evidence for the involvement of another tissue, skeletal muscle, in PARP2-elicited changes in lipid metabolism.

In addition to PARP2, other PARPs also play a role in cholesterol homeostasis. The ablation of PARP1 represses cholesterol efflux in macrophages by repressing LXR, resulting in repression of ABCA1 [38]. In hepatocytes, PARP1, together with histone H1.2, is vital for the efficient transcription of microsomal epoxide hydrolase (EPHX1), which facilitates bile acid export [39]. In addition, PARP1 activation has been linked to steroid-evoked changes [40-44]. A recent study suggests that PARP10 regulates lipid oxidation [45]. Apparently, PARPs have complex and widespread roles in regulating lipid metabolism.

The current study suggests that certain lipids can repress the expression of PARP2 and, therefore, PARP2 protein levels and activity. The first lipid species shown to inhibit PARP2 expression was α -lipoic acid [33]. Importantly, decreased PARP2 expression via α -lipoic acid had functional consequences, including enhanced SIRT1 activation [33]. Thus, α -lipoic acid may be a viable treatment supplement for obesity and type II diabetes [46-48]. Hereby, we add a set of cholesterol derivatives (dexamethasone, medroxyprogesterone acetate, tibolone, and oxandrolone) that have similar capabilities. These findings add a new modality to the regulation of PARP2 besides acetylation [49]. Note that PARP1 has lipid activators (7-ketocholesterol and fatty acids) [50, 51] and inhibitors (estrogen) [43], moreover, PARP1 deletion modulates the levels of several lipid species [52].

PARP2 has a partial protective effect on oxidative stress-related pathologies [11, 53, 54] and metabolic diseases, like obesity, type II diabetes, and hyperlipidemias [14, 18, 21], that is due to enhanced SIRT1 expression and the consequent mitochondrial biogenesis. Our current findings show that PARP2 has a role in regulating muscle strength and homeostasis; therefore, the activation of PARP2 can disrupt intramuscular endocrine homeostasis. Finally, as licensed PARP inhibitors block all enzymes in the PARP family, including PARP2 [55], the phenotype that we described may be a side effect of these inhibitors.

Materials and methods

Chemicals

All chemicals were from Sigma-Aldrich unless stated otherwise.

Cell culture

PARP2-silenced C2C12 cells were described in [18]. PARP2 knockdown and control clones were maintained over generations. C2C12 cells were cultured in DMEM (4500 mg/L glucose) (Sigma-Aldrich; Saint Louis, MO, USA) with 10% fetal calf serum (FCS). Cells were differentiated in DMEM (4500 mg/L glucose) containing 2% horse serum for 4 days in all experiments, except the luciferase reporter assays.

Animal studies

Homozygous PARP-2^{-/-} and littermate PARP-2^{+/+} male mice [28] on a C57BL/6J background, from heterozygous crossings were used. Animal experiments were approved by the Institutional Animal Care and Use Committee at the University of Debrecen and the National Board for Animal Experimentation (1/2014 DE MÁB). All animal experiments were carried out according to local, national, and EU ethical guidelines. Animal studies are reported in compliance with the ARRIVE guidelines [56]. Mice were killed by cervical dislocation. No more than six mice were housed in each cage (standard block shape = 365 × 207 × 140 mm, surface = 530 cm²; 1284 L Eurostandard Type II. L from Techniplast) with Lignocel Select Fine (J. Rettenmaier und Söhne, Germany) as bedding. Mice had paper tubes to enrich their environment. The dark/light cycle was 12 h, and temperature was 22 ± 1 °C. Cages were changed once a week, on the same day. Mice had ad libitum access to food and water (sterilized tap water). The animal facility was overseen by a veterinarian.

Cholesterol determination

Lipids were extracted from muscle and C2C12 cell samples by the Folch method, as described [57]. A cholesterol kit was used for the cholesterol quantitative determination (cholesterol RTU, bioMÉRIEUX; Marcy l'Etoile, France) following the recommendations of the manufacturer and adapted to a microplate format.

SDS-PAGE, Western blotting

Cells and tissues were lysed by RIPA buffer (50 mM Tris, 150 mM NaCl, 0.1 % SDS, 1% Nonidet P-40, 1 mM Na₃VO₃, 1 mM NaF, 0.5% sodium deoxycholate, 1 mM phenylmethylsulfonyl fluoride, protease inhibitor mixture; pH 8.0), then boiled with 2x Laemmli sample buffer and merkaptoethanol. Proteins were separated by SDS-PAGE on 8% acrylamide gels and transferred onto a nitrocellulose membrane (Amersham™ Protran® Supported, GE Healthcare; Chicago, IL, USA). Antibodies used in this study are shown in **Table 4**. The secondary antibody was anti-rabbit IgG POD (Sigma-Aldrich; St. Louis, MO,

USA). Labelled proteins were detected by an Alpha Innotech FluorChem FC2 device using a West Pico ECL Kit (Thermo Fisher Scientific; Waltham, MA, USA). Blots were quantified by densitometry using Image J software [58].

Cell fractionation

C2C12 cells transfected with scPARP2 or shPARP2 were washed with ice-cold PBS buffer and centrifuged at 4 °C at 100 g for 5 min. Pellets were (re)diluted in 4 volumes of homogenization buffer (0.5 M sucrose and 20 mM HEPES [pH 7.5]; 1 mM EDTA, 1 mM EGTA, protease inhibitors, and 0.5 % Nonidet-P) and were lysed and homogenized by aspirating through a 26-G needle 15 times. Lysates were centrifuged at 4 °C at 5000 g for 10 min. The supernatant was the cytosolic fraction, whereas the pellet was the nuclear fraction. To prepare the cytoplasmic fraction, the supernatant was centrifuged again at 8000 g at 4 °C for 3 min. The supernatant was used as a cytosolic fraction. To prepare the nuclear fraction, the pellet of the 5000-g centrifugation was resuspended in 3 volumes of 0.25 M sucrose, 10 mM Hepes (pH 7.9), 3.3 mM MgCl₂, 10 mM KCl, 0.5 mM DTT, and protease inhibitors and was lysed by passing through a 26-G needle 10 times; the lysate was subsequently spun at 4 °C at 2000 g for 15 min. The pellet was resolubilized in 0.35 M sucrose, 10 mM Hepes (pH 7.9), 3.3 mM MgCl₂, 10 mM KCl, 0.5 mM DTT, and protease inhibitors and was passed through a 26-G needle; it was then sonicated on ice (3x15 pulses, 15-s intervals). The sonicated suspension was regarded as the nuclear fraction.

Immunohistochemistry and confocal microscopy

Monolayer cells were grown on coverslips. Cells were washed with PBS and fixed in ice-cold methanol (air-dried). After fixation, the cells were rehydrated and permeabilized in 1% PBS_{TTX} followed by washes with PBS. Cells were incubated in blocking buffer (1 mg/ml BSA/PBS) for an hour at room temperature. After the blocking buffer was removed, cells were incubated with primary antibodies (SREBP1 1:100; SREBP2 1:100) (Santa Cruz; Santa Cruz, CA, USA) in 1 mg/ml BSA/PBS overnight using moist chambers (**Table 4.**). After the overnight incubation, cells were washed three times with PBS. For visualization, the secondary antibody, Alexa 488 FITC-conjugated anti-rabbit IgG (1:500) (Life Technologies; Carlsbad, CA, USA), was used. Nuclei were counterstained with ToPro-3 (1 μM final concentration) (Life Technologies). Cells were incubated with dyes for an hour at room temperature. Stained slides were assessed using a Leica TCS SP8 confocal microscope with a HC PL APO CS2 63x/1.40 oil immersion objective on a DMI6000 CS microscope. The confocal pictures were taken with LAS X 2.0.1.14392. software. Background fluorescence was determined from cells incubated with just the secondary antibody.

DNA constructs and luciferase activity measurement

Promoter transactivation was measured using a luciferase reporter assay. Cells were plated onto 6-well plates. Lipofectamine 3000 (Invitrogen, Thermo Fisher Scientific; Waltham, MA, USA) was used for transfection following the recommendations of the manufacturer. Co-transfection was performed with one of the following plasmids (4 µg): pGL2-SREBP1c-2600luc [59] for the study of the promoter of SREBP1, pKM2L-phSREBP2 (from the RIKEN Bioresource Center, Japan) for the study of the promoter of SREBP2, p-966 Star/hGH (generous gift from Barbara J. Clark; University of Louisville; Louisville, KY, USA) [60] for the study of the promoter of StAR, p-Luc-GW-Srd5a2 (-1500/+107) (generous gift from Timothy Osborne; Sanford-Burnham Medical Research Institute; Orlando, FL, USA) [61] for the study of the promoter of *srd5a* and 2 µg β-galactosidase expression plasmid (pCMV-βgal). Luciferase activity was measured by a Victor³ multilabel plate reader and normalized to β-galactosidase activity.

siRNA transfections

C2C12 cells were transfected with 30 nM Silencer Select siRNA (*Sreb1*, *Sreb2*; Thermo Fisher Scientific; Waltham, MA, USA) using Lipofectamine RNAiMAX transfection reagent (Thermo Fisher Scientific) for 48 h.

Microarray experiments and validation

Total RNA was extracted, using an RNeasy Mini Kit (Qiagen; Hilden, Germany), from C2C12 cells transfected with scPARP2 and shPARP2. RNA quality was assessed using Agilent Bioanalyser 2100 (Agilent Technologies; Santa Clara, CA, USA). The global expression pattern was analyzed on Affymetrix GeneChip Mouse Gene 1.0 ST array. Microarray experiments were performed as in [14]. Gene expressions profiles were validated by RT-qPCR as described later.

Lipid extraction and mass spectrometry

The solvents used for extraction and for mass spectrometry analyses were of liquid chromatographic grade (Merck; Darmstadt, Germany) and Optima LCMS grade (Thermo Fisher Scientific; Bremen, Germany). Lipid standards were obtained from Avanti Polar Lipids (Alabaster, AL, USA). All other chemicals were purchased from Sigma-Aldrich (Steinheim, Germany) and were of the best available grade.

For lipid extraction, C2C12 cells were washed twice with cold PBS, collected in Eppendorf tubes (6 million cells per tube), and centrifuged. The pellets were sonicated in a bath sonicator for 5 min in 1 mL methanol containing 0.001% butylated hydroxytoluene as an antioxidant, then shaken for 5 min and centrifuged at 10,000 × g for 5 min. The supernatant

was transferred into a new Eppendorf tube and stored at $-20\text{ }^{\circ}\text{C}$. For muscle samples, tissues were weighed and disrupted in water using a bullet blender homogenizer (Bullet Blender Gold, Next Advance; Location) in the presence of stainless steel beads (0.9-2 mm) at speed 10 for 7 min at $4\text{ }^{\circ}\text{C}$. Lipid extraction was carried out from a portion of the homogenate (ca. $10\text{ }\mu\text{L}$ corresponding to 2 mg w/w) in a similar fashion as for cell samples.

Mass spectrometric analyses were performed on a LTQ-Orbitrap Elite instrument (Thermo Fisher Scientific; Bremen, Germany) equipped with a robotic nanoflow ion source (TriVersa NanoMate; Advion BioSciences; Ithaca, NY, USA) as described in [62]. Orthogonal PLS-DA analyses of lipidomics datasets were performed using MetaboAnalyst [63].

RT-qPCR

Total RNA was isolated by Extrazol ready-to-use reagent (Blirt S. A.; Gdańsk, Poland). cDNA synthesis and RT-qPCR were performed as described in [14]. Expression was normalized to a geometric mean of 18S, cyclophilin or Gapdh. Primers are listed in **Table 3**.

Mechanical measurements in single permeabilized skeletal myofiber preparations

Gastrocnemius and diaphragm muscle tissue were obtained from PARP2^{+/+} and PARP2^{-/-} male mice. Tissue samples were snap-frozen and kept at -80°C until used. Muscle fibers were mechanically isolated from thawed samples in isolating solution (100 mM KCl , 2 mM EGTA , 1 mM MgCl_2 , $4\text{ mM Na}_2\text{ATP}$, 10 mM imidazole ; $\text{pH} = 7.0$) containing protease inhibitors ($0.5\text{ mM phenylmethylsulfonyl fluoride [PMSF]}$, $40\text{ }\mu\text{M leupeptin}$, and $10\text{ }\mu\text{M E-64}$; all from Sigma-Aldrich; St. Louis, MO, USA) at $4\text{ }^{\circ}\text{C}$. Muscle fibers were then permeabilized with 0.5% Triton X-100 detergent in the above solution for 4 min to remove all membranes. Single isolated and skinned muscle fibers were mounted between two stainless insect needles with silicone adhesive (DAP 100% all-purpose silicone sealant; Baltimore, MD, USA) at $15\text{ }^{\circ}\text{C}$. The needles were connected to a highly sensitive force transducer (Sensonor; Horten, Norway) and an electromagnetic length controller (Aurora Scientific Inc.; Aurora, Canada). Activating and relaxing solutions were used during force measurements. The activating solution with the highest Ca^{2+} concentration contained $7\text{ mM Ca}^{2+}\text{-EGTA}$, 37.34 mM KCl , $10\text{ mM N,N-bis (2-hydroxyethyl)-2-aminoethanesulfonic acid (BES)}$, 6.24 mM MgCl_2 , $6.99\text{ mM Na}_2\text{ATP}$, $15\text{ mM Na}_2\text{CrP}$ ($\text{pH} = 7.2$, $\text{pCa } 4.75$) (Ca^{2+} concentrations are expressed in logarithmic units [pCa]). The relaxing solution contained the same components as above except it included EGTA instead of $\text{Ca}^{2+}\text{-EGTA}$ ($\text{pH} = 7.2$; $\text{pCa} = 9$). Both solutions were supplemented with protease inhibitors as above. Solutions with intermediate Ca^{2+} concentrations were prepared by mixing activating and relaxing solutions ($\text{pCa} = 5.4\text{-}7.0$).

Active force (F_{active}) and Ca^{2+} -sensitivity to force production (pCa_{50}) were determined in activating solutions with different Ca^{2+} concentrations. When active muscle force reached its

maximum, a quick release-restretch maneuver (30 ms) was applied in activating solution. Due to this maneuver, force first dropped from the peak isometric level to 0 (total peak isometric force, F_{total}) and then it started to redevelop. Fiber type was identified on the basis of force redevelopment kinetics following the quick release-restretch maneuvers. Ca^{2+} -independent passive force (F_{passive}) was approximated by shortening the preparations to 80% of the original lengths in relaxing solution for 8 s. Active isometric force (F_{active}) was calculated as the difference between F_{total} and F_{passive} . Preparations were exposed to a series of solutions with intermediate Ca^{2+} concentrations to construct pCa-force relationships. Lastly, preparations were exposed to an activating solution with saturating Ca^{2+} concentration (pCa = 4.75); and if maximal isometric force (F_{max}) at this time was less than 80% of the initial F_{max} , the experiment was discarded. F_{active} at submaximal Ca^{2+} levels was normalized to F_{max} (pCa 4.75, F_{max}). The relation between the F_{active} and pCa was fitted to a modified Hill equation: $F = F_{\text{max}}[\text{Ca}^{2+}]^{n_{\text{Hill}}}/(\text{Ca}_{50}^{n_{\text{Hill}}} + [\text{Ca}^{2+}]^{n_{\text{Hill}}})$ where F was the force at a given Ca^{2+} concentration ($[\text{Ca}^{2+}]$), F_{max} , n_{Hill} and pCa_{50} denoted the maximal F_{active} at saturating $[\text{Ca}^{2+}]$ and the slope and the midpoint of the sigmoidal relationship, respectively. Absolute forces (F_{active} and F_{passive}) were normalized to a cross-sectional area and expressed in kN/m^2 . Sarcomere length (SL) was adjusted to 2.3 μm . Ca^{2+} -evoked contractures were recorded by a custom-built LABVIEW Data Acquisition platform and analyzed by a LabVIEW analyzing software (Myo; National Instruments; Austin, TX, USA).

Muscular steroid hormone extraction and determination

Steroid extraction was performed similarly to [64]. DHT, testosterone, and androstenedione were measured by an RIA kit (Beckman Coulter; Brea, CA, USA). Testosterone and androstenedione were determined from whole skeletal muscle of a mouse. For the measurement of DHT, a pool of gastrocnemius muscle was used from PARP2 wild-type and from PARP2 knockout mice; hence, we cannot determine the biological error.

ImFCS

Cells were seeded into glass bottom dishes (MatTek Corporation; City, MA, USA) a day before the experiments. After labeling the cells with fluorescent lipid probe (BODIPY FL C5-sphingomyelin; Molecular Probes; Eugene, OR, USA) for 8 min at 37 °C, cells were washed three times with the culture media. The measurements were performed in culture media without phenol red, in a POC-R cell cultivation system (Zeiss; Jena, Germany). This system incorporates a controlled objective heater and CO_2 /air gas chamber. Objective-type TIRF illumination was used to achieve the thinnest excited sample volume, with a high numerical aperture objective (alpha Plan-FLUAR 100; Zeiss). The data were acquired using a ProEM512 EMCCD camera (Princeton Instruments; Trenton, NJ, USA) with a 3-ms effective

exposure time and a 20 × 40 pixel acquisition area per measurement (pixel size = 0.16 μm). The ImFCS plugin for ImageJ software was used for data evaluation (http://www.dbs.nus.edu.sg/lab/BFL/imfcs_image_j_plugin.html). Detailed data analysis is described in [62].

Chip-seq reanalysis

We investigated 32 publicly available ChIP-seq data in nine different human and mouse cell types (GEO identifiers and references are in **Table 5, 6**). The human experiments were performed in two lymphoblastoid cell lines (GM10855 and GM10861), in leukemia monocytic (THP-1), hepatic stellate (LX2) and prostate cancer (LNCaP) cells. The mouse ChIP-seq data were derived from mouse intestinal epithelial cells, from osteoblast precursor (MC3T3-E1) cell line and from non-differentiated (MSC), osteogenic (MSC osteogenic) or adipogenic (MSC adipogenic) differentiation media-treated bone marrow-derived mesenchymal stem cells (MSC).

Raw sequence data were aligned to the mm10 reference genome assembly by using the Burrows-Wheeler Alignment (BWA) tool (v0.7.10) [65]. BAM files were generated by SAM tools (v0.1.19) [66], and BEDGRAPH files were created by the makeUCSCfile of Hypergeometric Optimization of Motif EnRichment (HOMER) tool (v4.2) [67]. Peaks were predicted with MACS2 [68], and coverage files were also created by HOMER.

The equivalent DNA sequences of the Vitamin D response element (VDRE) at human PARP1 gene promoter could be identified in 37 different species based on the Comparative Genomics data sets of Ensembl database (Archive Ensembl 75: GRCh17.p13). Sequence of the VDRE ±10 base pairs was visualized by using BioEdit Sequence Alignment Editor (v7.0.5.3) [69].

Database screening

The GEO (profiles) database of the NCBI was screened for PARP2+steroid and PARP2+lipid keywords.

Data availability

The primary data of the present manuscript are available at <https://figshare.com/s/3e7866c3ce9db7c4df88>. The microarray dataset has been uploaded to the Geo database of NCBI at GSE108737.

Statistical analysis

For the comparison of two groups, we used the two-tailed, unpaired Student's *t*-test. *p* values smaller than 0.05 were considered significant. Significance levels were given in the

figure captions, actual p values can be found in the primary dataset available online (<https://figshare.com/s/3e7866c3ce9db7c4df88>). Actual p values are given for those comparisons, where p is slightly higher than 0.05.

Acknowledgements

The authors are grateful to Mr. László Finta for technical assistance and to Dr. Pál Gergely (Department of Medical Chemistry, University of Debrecen) for valuable discussions.

Our work was financed by the K123975, PD121138, K120669, PROJEKT2017-44, GINOP-2.3.2-15-2016-00006, EFOP-3.6.3-VEKOP-16-2017-00009 and EFOP-3.6.2-16-2017-00006 grants from the NKFIH. MS is a recipient of the Bolyai fellowship of the Hungarian Academy of Sciences, BB is a recipient of the ÚNKP-17-3-IV-DE-96 New National Excellence Program grant of the Ministry of Human Capacities, BLB and DB were supported by the MOLMEDEX FUN-OMICS (GINOP-2.3.3-15-2016-00007) and Debrecen Venture Catapult Program (EFOP-3.6.1-16-2016-00022). Grants were implemented through the New Hungary Development Plan co-financed by the European Social Fund and the European Regional Development Fund.

Author contributions

Performed experiments: JM, AV, MS, LJ

Lipidomics: MP, GB, IH, LV

ImFCS: IG, ZT, LV

Hormone determination: HBP

Force measurement: BB, ZP

In silico assessment: DB, BLB

Wrote the manuscript: JM, KU, HBP, ZP, LV, PB

Conflict of interest

The authors declare that they have no conflict of interest.

References

1. Ame, JC, C Spenlehauer, and G de Murcia, *The PARP superfamily*. Bioessays, 2004. **26**(8): p. 882-893.
2. Hottiger, MO, et al., *Toward a unified nomenclature for mammalian ADP-ribosyltransferases*. Trends Biochem Sci, 2010. **35**(4): p. 208-219.
3. Leger, K, et al., *ARTD2 activity is stimulated by RNA*. Nucleic Acids Res, 2014. **42**(8): p. 5072-5082.
4. Kutuzov, MM, et al., *Interaction of PARP-2 with DNA structures mimicking DNA repair intermediates and consequences on activity of base excision repair proteins*. Biochimie, 2013. **95**(6): p. 1208-1215.

5. Kutuzov, MM, et al., *Interaction of PARP-2 with AP site containing DNA*. Biochimie., 2015. **112**: p. 10-19.
6. Sukhanova, MV, et al., *Single molecule detection of PARP1 and PARP2 interaction with DNA strand breaks and their poly(ADP-ribosyl)ation using high-resolution AFM imaging*. Nucleic Acids Res, 2016. **44**(6): p. e60.
7. Ame, JC, et al., *PARP-2, A novel mammalian DNA damage-dependent poly(ADP-ribose) polymerase*. J Biol Chem, 1999. **274**(25): p. 17860-17868.
8. Schreiber, V, et al., *Poly(ADP-ribose): novel functions for an old molecule*. Nat Rev Mol Cell Biol, 2006. **7**(7): p. 517-528.
9. Bai, P, *Biology of Poly(ADP-Ribose) Polymerases: The Factotums of Cell Maintenance*. Mol Cell, 2015. **58**(6): p. 947-958.
10. Schreiber, V, et al., *Poly(ADP-ribose) polymerase-2 (PARP-2) is required for efficient base excision DNA repair in association with PARP-1 and XRCC1*. J Biol Chem, 2002. **277**(25): p. 23028-23036.
11. Szanto, M, et al., *Poly(ADP-ribose) polymerase-2 depletion reduces doxorubicin-induced damage through SIRT1 induction*. Cardiovasc Res, 2011. **92**(3): p. 430-8.
12. Dantzer, F, et al., *Poly(ADP-ribose) polymerase-2 contributes to the fidelity of male meiosis I and spermiogenesis*. Proc Natl Acad Sci U S A, 2006. **103**(40): p. 14854-14859.
13. Frizzell, KM, et al., *Global analysis of transcriptional regulation by poly(ADP-ribose) polymerase-1 and poly(ADP-ribose) glycohydrolase in MCF-7 human breast cancer cells*. J Biol Chem, 2009. **284**(49): p. 33926-33938.
14. Szántó, M, et al., *Deletion of PARP-2 induces hepatic cholesterol accumulation and decrease in HDL levels*. Biochem Biophys Acta - Molecular Basis of Disease, 2014. **1842**(4): p. 594-602.
15. Bai, P, et al., *Poly(ADP-ribose) polymerase-2 controls adipocyte differentiation and adipose tissue function through the regulation of the activity of the retinoid X receptor/peroxisome proliferator-activated receptor-gamma heterodimer*. J Biol Chem, 2007. **282**(52): p. 37738-37746.
16. Maeda, Y, et al., *PARP-2 interacts with TTF-1 and regulates expression of surfactant protein-B*. J Biol Chem, 2006. **281**(14): p. 9600-9606.
17. Farres, J, et al., *PARP-2 is required to maintain hematopoiesis following sublethal gamma-irradiation in mice*. Blood, 2013. **122**(1): p. 44-54.
18. Bai, P, et al., *PARP-2 regulates SIRT1 expression and whole-body energy expenditure*. Cell Metab, 2011. **13**(4): p. 450-460.
19. Yelamos, J, V Schreiber, and F Dantzer, *Toward specific functions of poly(ADP-ribose) polymerase-2*. Trends Mol Med, 2008. **14**(4): p. 169-178.
20. Yelamos, J, et al., *PARP-2 deficiency affects the survival of CD4+CD8+ double-positive thymocytes*. EMBO J, 2006. **25**(18): p. 4350-4360.
21. Mohamed, JS, et al., *MicroRNA-149 inhibits PARP-2 and promotes mitochondrial biogenesis via SIRT-1/PGC-1alpha network in skeletal muscle*. Diabetes, 2014. **63**(5): p. 1546-59.
22. Filliol, A, et al., *PARP2 deficiency affects invariant-NKT-cell maturation and protects mice from concanavalin A-induced liver injury*. Am J Physiol Gastrointest Liver Physiol, 2017. **313**(5): p. G399-G409.
23. Szanto, M, et al., *Poly(ADP-ribose) polymerase-2: emerging transcriptional roles of a DNA-repair protein*. Cell Mol Life Sci, 2012. **69**(24): p. 4079-92.
24. Farres, J, et al., *PARP-2 sustains erythropoiesis in mice by limiting replicative stress in erythroid progenitors*. Cell Death Differ, 2015. **22**(7): p. 1144-1157.
25. Bai, P and C Canto, *The role of PARP-1 and PARP-2 enzymes in metabolic regulation and disease*. Cell Metab, 2012. **16**(5): p. 290-295.
26. Vida, A, et al., *Metabolic roles of poly(ADP-ribose) polymerases*. Semin Cell Dev Biol., 2017. **63**: p. 135-143.
27. Manunza, A, et al., *A genome-wide association analysis for porcine serum lipid traits reveals the existence of age-specific genetic determinants*. BMC Genomics, 2014. **15**: p. 758.

28. Menissier-de Murcia, J, et al., *Functional interaction between PARP-1 and PARP-2 in chromosome stability and embryonic development in mouse*. EMBO J, 2003. **22**(9): p. 2255-2263.
29. Brown, MS and JL Goldstein, *The SREBP pathway: regulation of cholesterol metabolism by proteolysis of a membrane-bound transcription factor*. Cell, 1997. **89**(3): p. 331-340.
30. Tang, JJ, et al., *Inhibition of SREBP by a small molecule, betulin, improves hyperlipidemia and insulin resistance and reduces atherosclerotic plaques*. Cell Metab, 2011. **13**(1): p. 44-56.
31. Sato, K and M Iemitsu, *Exercise and sex steroid hormones in skeletal muscle*. J Steroid Biochem Mol Biol, 2015. **145**: p. 200-205.
32. Ng, XW, N Bag, and T Wohland, *Characterization of lipid and cell membrane organization by the fluorescence correlation spectroscopy diffusion law*. Chim Int J Chem, 2015. **39**: p. 112-119.
33. Zhang, L, et al., *Alpha-lipoic acid attenuates cardiac hypertrophy via downregulation of PARP-2 and subsequent activation of SIRT-1*. Eur J Pharmacol, 2014. **744**: p. 203-210.
34. Gene Expression Omnibus: Dexamethasone PARP2. Date accessed: 2017. 11. 04. https://www.ncbi.nlm.nih.gov/geo/tools/profileGraph.cgi?ID=GDS2314:1417800_at
35. Gene Expression Omnibus: Medroxyprogesterone acetate, tibolone PARP2. Date accessed: 2017. 11. 04. https://www.ncbi.nlm.nih.gov/geo/tools/profileGraph.cgi?ID=GDS3313:214086_s_at
36. Gene Expression Omnibus: Oxandrolone PARP2. Date accessed: 2017. 11. 04. https://www.ncbi.nlm.nih.gov/geo/tools/profileGraph.cgi?ID=GDS1333:214086_s_at
37. Hagen, RM, S Rodriguez-Cuenca, and A Vidal-Puig, *An allostatic control of membrane lipid composition by SREBP1*. FEBS Lett, 2010. **584**(12): p. 2689-2698. .
38. Shrestha, E, et al., *Poly(ADP-ribose) polymerase 1 represses liver X receptor-mediated ABCA1 expression and cholesterol efflux in macrophages*. J Biol Chem, 2016. **291**(21): p. 11172-11184.
39. Peng, H, et al., *Transcription of the human microsomal epoxide hydrolase gene (EPHX1) Is regulated by PARP-1 and Histone H1.2. Association with sodium-dependent bile acid transport*. PLoS One., 2015. **10**(5): p. e0125318.
40. Shi, L, et al., *Loss of androgen receptor in aging and oxidative stress through Myb protooncoprotein-regulated reciprocal chromatin dynamics of p53 and poly(ADP-ribose) polymerase PARP-1*. J Biol Chem., 2008. **283**(52): p. 36474-85.
41. Pu, H, et al., *PARP-1 regulates epithelial-mesenchymal-transition (EMT) in prostate tumorigenesis*. Carcinogenesis, 2014. **35**(11): p. 2592-2601.
42. Masszi, G, et al., *Reduced estradiol-induced vasodilation and poly-(ADP-ribose) polymerase (PARP) activity in the aortas of rats with experimental polycystic ovary syndrome (PCOS)*. PLoS One, 2013. **8**(3): p. e55589.
43. Mabley, JG, et al., *Gender differences in the endotoxin-induced inflammatory and vascular responses: potential role of poly(ADP-ribose) polymerase activation*. J Pharmacol Exp Ther, 2005. **315**(2): p. 812-820.
44. Shimizu, T, et al., *Androgen and PARP-1 regulation of TRPM2 channels after ischemic injury*. J Cereb Blood Flow Metab, 2013. **33**(10): p. 1549-1555.
45. Marton, J, et al., *PARP10 (ARTD10) modulates mitochondrial function*. PLoS One, 2018. **13**(1): p. e0187789.
46. Kucukgoncu, S, et al., *Alpha-lipoic acid (ALA) as a supplementation for weight loss: results from a meta-analysis of randomized controlled trials*. Obes Rev, 2017. **18**(5): p. 594-601.
47. Namazi, N, B Larijani, and L Azadbakht, *Alpha-lipoic acid supplement in obesity treatment: A systematic review and meta-analysis of clinical trials*. Clin Nutr, 2017. **37**(2): p. 419-428.
48. Rochette, L, et al., *Alpha-lipoic acid: molecular mechanisms and therapeutic potential in diabetes*. Can J Physiol Pharmacol, 2015. **93**(12): p. 1021-1027.
49. Haenni, SS, et al., *Identification of lysines 36 and 37 of PARP-2 as targets for acetylation and auto-ADP-ribosylation*. Int J Biochem Cell Biol, 2008. **40**(10): p. 2274-2283.

50. Diestel, A, et al., *Activation of microglial poly(ADP-ribose)-polymerase-1 by cholesterol breakdown products during neuroinflammation: a link between demyelination and neuronal damage*. J Exp Med, 2003. **198**(11): p. 1729-1740.
51. Chen, Y, et al., *Acyl-CoA-binding domain containing 3 modulates NAD⁺ metabolism through activating poly(ADP-ribose) polymerase 1*. Biochem J, 2015. **469**(2): p. 189-198.
52. Kiss, B, et al., *Poly(ADP) ribose polymerase-1 ablation alters eicosanoid and docosanoid signaling and metabolism in a murine model of contact hypersensitivity*. Mol Med Rep, 2015. **11**(4): p. 2861-2867.
53. Li, X, et al., *Contributions of poly(ADP-ribose) polymerase-1 and -2 to nuclear translocation of apoptosis-inducing factor and injury from focal cerebral ischemia*. J Neurochem, 2010. **113**(4): p. 1012-1022.
54. Kofler, J, et al., *Differential effect of PARP-2 deletion on brain injury after focal and global cerebral ischemia*. J Cereb Blood Flow Metab, 2006. **26**(1): p. 135-141.
55. Wahlberg, E, et al., *Family-wide chemical profiling and structural analysis of PARP and tankyrase inhibitors*. Nat Biotechnol, 2012. **30**(3): p. 283-288.
56. McGrath, JC, et al., *Guidelines for reporting experiments involving animals: the ARRIVE guidelines*. Br J Pharmacol, 2010. **160**(7): p. 1573-1576.
57. Folch, J, M Lees, and GH Sloane Stanley, *A simple method for the isolation and purification of total lipides from animal tissues*. J Biol Chem, 1957. **226**(1): p. 497-509.
58. Rueden, CT, et al., *ImageJ2: ImageJ for the next generation of scientific image data*. BMC Bioinformatics, 2017. **18**(1): p. 529.
59. Hasty, AH, et al., *Sterol regulatory element-binding protein-1 is regulated by glucose at the transcriptional level*. J Biol Chem, 2000. **275**(40): p. 31069-31077.
60. Caron, KM, et al., *Characterization of the promoter region of the mouse gene encoding the steroidogenic acute regulatory protein*. Mol Endocrinol, 1997. **11**(2): p. 138-147.
61. Seo, YK, et al., *Regulation of steroid 5-alpha reductase type 2 (Srd5a2) by sterol regulatory element binding proteins and statin*. Exp Cell Res, 2009. **315**(18): p. 3133-3139.
62. Peksel, B, et al., *Mild heat induces a distinct "eustress" response in Chinese Hamster Ovary cells but does not induce heat shock protein synthesis*. Sci Rep., 2017. **7**(1): p. 15643.
63. Xia, J and DS Wishart, *Using metaboAnalyst 3.0 for comprehensive metabolomics data analysis*. Curr Protoc Bioinformatics, 2016: p. doi: 10.1002/cpbi.11.
64. Marks, LS, et al., *Tissue effects of saw palmetto and finasteride: use of biopsy cores for in situ quantification of prostatic androgens*. Urology, 2001. **57**(5): p. 999-1005.
65. Li, H and R Durbin, *Fast and accurate short read alignment with Burrows-Wheeler transform*. Bioinformatics, 2009. **25**(14): p. 1754-1760.
66. Li, H, et al., *The sequence alignment/map format and SAMtools*. Bioinformatics, 2009. **25**(16): p. 2078-2079.
67. Heinz, S, et al., *Simple combinations of lineage-determining transcription factors prime cis-regulatory elements required for macrophage and B cell identities*. Mol Cell, 2010. **38**(4): p. 576-589.
68. Zhang, Y, et al., *Model-based analysis of ChIP-Seq (MACS)*. Genome Biol, 2008. **9**(9): p. R137. .
69. Hall, TA, *BioEdit: a user-friendly biological sequence alignment editor and analysis program for Windows 95/98/NT*. . Nucl Acids Symp Ser, 1999. **41**: p. 95-98.
70. Novodata Pharmed. Date accessed: 2018. 07. 10. <http://www.novodata.hu/pharmainfo>
71. Miko, E, et al., *Lithocholic acid, a bacterial metabolite reduces breast cancer cell proliferation and aggressiveness*. Biochim Biophys Acta, 2018: p. doi: 10.1016/j.bbabo.2018.04.002.
72. Halperin, G, et al., *A new method for determination of serum cholestanol by high-performance liquid chromatography with ultraviolet detection*. J Chromatogr B Biomed Sci Appl, 2000. **742**(2): p. 345-352.
73. Department of Laboratory Medicine, University of Debrecen: Reference ranges of laboratory analytes. Date accessed: 2018. 07. 10. <http://labmed.hu/v/vall.php#>

74. Pirke, KM and P Doerr, *Plasma dihydrotestosterone in normal adult males and its relation to testosterone*. Acta Endocrinol (Copenh), 1975. **79**(2): p. 357-365.

Figure legends

Figure 1. Silencing of PARP2 induces changes to the lipidome.

- A.** PARP2 levels were determined by RT-qPCR in C2C12 cells transfected with scPARP2 or shPARP2 (n = 4, in triplicates) and in the skeletal muscle of PARP2^{+/+} and PARP2^{-/-} male mice (3 months of age, n = 9/8). Protein levels of PARP2 were detected by Western blotting in the same cohorts of C2C12 cells and mice. Actin was used as a loading control.
- B.** OPLS-DA score plots of lipidomic datasets (n = 4 for scPARP2 vs. shPARP2 C2C12 cells, and n = 12/8 for PARP2^{+/+} vs. PARP2^{-/-} skeletal muscles).

All abbreviations are in the text. (A) The two-tailed, unpaired Student's *t*-test was used for comparisons. *, **, and *** represent statistically significant differences between the scPARP2 and shPARP2 C2C12 cells or PARP2^{+/+} and PARP2^{-/-} mice at p < 0.05, 0.01, and 0.001, respectively. Averages of values are presented. For cell studies, error is represented as ± SD; for murine studies, error is represented as ± SEM. (B) The OPLS-DA model was validated by permutation tests.

Figure 2. Silencing of PARP2 induces the expression of SREBP1, SREBP2, and their target genes.

- A.** Gene expression was analyzed in scPARP2 and shPARP2 C2C12 cells (n = 1, in triplicates) using microarray, and genes were selected as a function of their biological function.
- B.** Microarray data were validated by RT-qPCR using RNA prepared from scPARP2 and shPARP2 C2C12 cells (n = 3, in triplicates) and RNA prepared from the gastrocnemius muscle of PARP2^{+/+} and PARP2^{-/-} male mice (3 months of age, n = 8/8). The indicated genes were assessed.
- C.** The transactivation of the promoter of SREBP1 and 2 was assessed in luciferase reporter assays in scPARP2 and shPARP2 C2C12 cells (n = 3, in duplicates for both promoters).
- D-E.** SREBP1 and SREBP2 were silenced in scPARP2 and shPARP2 C2C12 cells (n = 3/3). Undifferentiated C2C12 cells were transfected with siRNA for 2 days; then (D) the indicated proteins were determined by Western blotting, and (E) HMGR mRNA expression was determined by RT-qPCR.

All abbreviations are in the text. The two-tailed, unpaired Student's *t*-test was used for comparisons, except for panel E, where two-way ANOVA with the Tukey post-hoc test was used. Statistically significant differences between the scPARP2 and shPARP2 C2C12 cells or PARP2^{+/+} and PARP2^{-/-} mice are represented as *, **, and *** for $p < 0.05$, 0.01, and 0.001, respectively. Average values are presented, and error is represented as \pm SEM.

Figure 3. Silencing of PARP2 activates SREBP1 and SREBP2.

- A. In C2C12 cells transfected with scPARP2 and shPARP2 ($n = 3/3$; left side) and in the gastrocnemius muscle of PARP2^{+/+} and PARP2^{-/-} male mice (right; 3 months of age, $n = 7/11$), the indicated proteins were assessed by Western blotting. Actin was used as a loading control. Representative blots are presented.
- B. The cellular localizations of SREBP1 and SREBP2 were assessed by fluorescence immunocytochemistry and confocal microscopy in scPARP2 and shPARP2 C2C12 cells ($n = 1$, 9/9 cells were assessed). One characteristic sample is shown. The ratio between the nuclear and extranuclear SREBP1 and 2 was calculated. Scale bar: 25 μ m.
- C. The expressions of the indicated genes were measured by qRT-qPCR in the mRNA pool of scPARP and shPARP2 C2C12 cells ($n = 2$).
- D. In scPARP2 and shPARP2 C2C12 cells ($n = 1$), the expressions of SREBP1 and SREBP2 were assessed after 48 h of treatment with 10 μ g/ml betulin.
- E. Cholesterol was determined in scPARP2 and shPARP2 C2C12 cells ($n = 3/3$, in triplicates) and in gastrocnemius muscle of PARP2^{+/+} and PARP2^{-/-} male mice (3 months of age, $n = 7/11$). Cholesterol concentration is given as μ g cholesterol/mg cell pellet for cell samples or μ g/mg wet weight for muscles.

All abbreviations are in the text. The two-tailed, unpaired Student's *t*-test was used for comparisons. Statistically significant differences between the scPARP2 and shPARP2 C2C12 cells or PARP2^{+/+} and PARP2^{-/-} mice are represented as *, **, and *** for $p < 0.05$, 0.01, and 0.001, respectively. Average values are presented, and error is represented as \pm SEM.

Figure 4. Silencing of PARP2 induces anabolic steroid synthesis in the skeletal muscle.

- A. mRNA expression levels of *Star*, *Hsd17b11*, *Srd5a1*, and *Srd5a2* in scPARP2 and shPARP2 C2C12 cells ($n = 3$, in triplicates) and in gastrocnemius muscle of PARP2^{+/+} and PARP2^{-/-} male mice (3 months of age, $n = 13/10$) quantified by RT-qPCR.

- B.** The activity of the Star and Srd5a1 promoter was assessed in scPARP2 and shPARP2 C2C12 cells (n = 3/3) using luciferase reporter assays.
- C.** Steroid concentrations were measured by RIA assays in skeletal muscle of PARP2^{+/+} and PARP2^{-/-} male mice (3 months of age, n = 18/18). For testosterone and androstenedione measurements, all skeletal muscles were harvested from mice and extracted. For DHT, the gastrocnemius muscles were harvested from all mice in the study.

All abbreviations are in the text. The two-tailed, unpaired Student's *t*-test was used for comparisons. Statistically significant differences between the scPARP2 and shPARP2 C2C12 cells or PARP2^{+/+} and PARP2^{-/-} mice are represented as *, **, and *** for $p < 0.05$, 0.01, and 0.001, respectively. Averages of values are presented, and error is represented as \pm SEM. The values of the DHT levels represent mixtures derived from gastrocnemius muscles of PARP2^{+/+} and PARP2^{-/-} male mice, respectively. Therefore, we did not perform statistical analysis.

Figure 5. Genetic deletion of PARP2 augments skeletal muscle fiber strength.

Skeletal myofibers were isolated from gastrocnemius muscle (**left**; n = 7/7 for slow-twitch and n = 9/7 for fast-twitch fibers, all from different animals) or from the diaphragm (**right**; n = 3/4 for slow- and n = 3/3 for fast-twitch fibers, all from different animals) of 3-mo-old PARP2^{+/+} or PARP2^{-/-} male mice. Ca²⁺-independent passive force (F_{passive}) of permeabilized muscle fibers was determined in relaxing solution (pCa = 9.0) (**A**). The upper parts of panel **B** depict the Ca²⁺-dependence of active force productions (F_{active}), and bar graphs at the bottom illustrate maximal Ca²⁺-activated active force values (F_{max} , pCa = 4.75) in PARP2^{+/+} and PARP2^{-/-} male mice for the gastrocnemius and diaphragm muscles. To determine the Ca²⁺-sensitivity of force production (pCa₅₀, insets), F_{active} values at submaximal levels of activations were normalized to F_{max} (**C**). All abbreviations are given in the text. The two-tailed, unpaired Student's *t*-test was used for comparisons. Data are expressed as mean \pm SEM. Statistically significant differences between the control values vs. calcium treatment are represented as * for $p < 0.05$. Statistically significant differences between muscles of PARP2^{+/+} and PARP2^{-/-} mice are represented as # for $p < 0.05$.

Figure 6. Silencing of PARP2 modifies the lateral diffusion properties of the SM-probe in the plasma membrane.

In scPARP2 and shPARP2 C2C12 cells, the diffusion of the BODIPY FL-SM probe (n = 36) was assessed. The average of D (**A**) and τ_0 values (**B**) are depicted (\pm SEM). The two-tailed, unpaired Student's *t*-test was used for comparisons. Statistical significance between scPARP2 and shPARP2 C2C12 cells at $p < 0.05$ is represented as *.

Figure 7. Vitamin D receptor is bound to a vitamin D response element (VDRE) at the promoter of PARP2.

- A. Vitamin D receptor (VDR) peaks were identified in available ChIP-seq data as described.
- B. VDREs were identified on the promoter of PARP2 in different species.

Figure 8. Lipid species can modulate the expression of PARP2.

- A. C2C12 cells were treated with vitamin D in the concentrations indicated for 48 h; then protein levels of PARP2 and VDR were determined by Western blotting (n = 2).
- B. C2C12 cells were treated with the lipid species in the concentrations indicated for 48 h; then PARP2 levels were assessed by Western blotting (n = 2).

The two-tailed, unpaired Student's *t*-test was used for comparisons. Data are expressed as mean \pm SEM; * and ** represent statistical significance at $p = 0.05$ or 0.01 between vehicle and drug-treated C2C12 cells, respectively. Abbreviations are in Table 2.

Table 1. Functional grouping of dysregulated genes in scPARP2 vs. shPARP2 C2C12 cells.

Genes with a fold change of 1.5, or larger are shown. *, ** and *** indicate statistically significant differences between scPARP2 and shPARP2 cells at $p < 0.05$, $p < 0.01$ and $p < 0.001$, respectively.

	Upregulated genes		Downregulated genes	
Muscular function	Name	Fold	Name	Fold
	<i>Tnni1</i>	2.18x**	<i>Alcam</i>	-2.37x*
	<i>Tnnc1</i>	2.49x**	<i>Actg2</i>	-2.21x*
	<i>Myh10</i>	2.40x**	<i>Cxcr4</i>	-2.20x**
	<i>Tnnt2</i>	3.26x**	<i>Etv1</i>	-4.51x***
	<i>Tnnt3</i>	2.17x**	<i>Gja1</i>	-2.31x*
	<i>Acta1</i>	2.33x**	<i>Lama2</i>	-4.41x**
	<i>Actn3</i>	2.62x*	<i>Itgb3</i>	-4.48x**
	<i>Atp1a2</i>	2.11x*	<i>Musk</i>	-3.63x*
	<i>Artn</i>	2.53x*	<i>Mef2c</i>	-2.51x**
	<i>Cspg4</i>	3.52x**	<i>Met</i>	-2.60x*
	<i>Cd34</i>	5.81x**	<i>Mbnl3</i>	-3.36x**
	<i>Flnb</i>	2.36x*	<i>Robo2</i>	-5.08x**
	<i>Kif5c</i>	3.38x**	<i>Robo1</i>	-4.63x**
	<i>Myom2</i>	2.42x*	<i>Sema5a</i>	-2.01x*
	<i>Mylpf</i>	2.32x**	<i>Tns1</i>	-1.94x*
	<i>Myf5</i>	2.18x*	<i>Tns3</i>	-2.29x**
	<i>Mospd2</i>	2.08x**		
	<i>Prkca</i>	2.42x**		
	<i>Pdpr</i>	2.78x**		
	<i>Tnc</i>	5.08x**		
	<i>Unc5c</i>	1.03x*		
Lipid metabolism	<i>Stard4</i>	2.44x**	<i>Acox2</i>	-2.53x*
	<i>Hmgcs1</i>	3.38x**	<i>Cerk</i>	-2.37x**
	<i>Ldlr</i>	3.08x***	<i>Il1rn</i>	-4.33x**
	<i>Hsd17b7</i>	4.56x**	<i>Pcx</i>	-2.60x**
	<i>Hmgcr</i>	2.26x*	<i>Prkar2b</i>	-3.65x*
	<i>Acot10</i>	2.16x**	<i>Pla2g7</i>	-6.49x**
	<i>Cyp51</i>	3.43x**	<i>Plcb1</i>	-3.96x**

	<i>Dhcr7</i>	2.30x*		
	<i>Dhcr24</i>	2.05x*		
	<i>Idi1</i>	3.99x**		
	<i>Lss</i>	2.84x**		
	<i>Nsdhl</i>	2.19x**		
	<i>Pmvk</i>	2.64x*		
	<i>Pcsk9</i>	2.96x**		
	<i>Sc4mol</i>	3.25x**		
	<i>Sc5d</i>	2.26x**		
	<i>Tm7sf2</i>	2.89x**		
	<i>Alox5</i>	2.25x*		
	<i>Lass4</i>	2.55x*		
	<i>Ptgis</i>	2.52x*		
	<i>Pcyt2</i>	2.18x*		
	<i>Smpd3</i>	2.04x*		

Table 2. List of lipid compound used to modulate PARP2 expression

Name	Human reference/therapeutic range	Concentration in the study	Reference
Medroxyprogesterone-acetate (MPA)	up to 7 nM	30 nM	[71]
Tibolone	32 - 48 nM	30 nM	[71]
Dexamethasone (DEX)	20,4 μ M	10 μ M	[71]
Cholic acid (CA)	0.48 – 2 μ M	2 μ M	[72]
Chenodeoxycholic acid (CDCA)	0.32 – 2.2 2 μ M	2 2 μ M	[72]
Lithocholic acid (LCA)	10 – 50 nM	50 nM	[72]
Deoxycholic acid (DCA)	0.7 – 1 μ M	1 μ M	[72]
Ursodeoxycholic acid (UDCA)	100 – 300 nM	300 nM	[72]
Cholestanol (CHOL)	9.26 \pm 5.4 μ M	14 μ M	[73]
Trans-dehydroepiandrosterone (DHEA)	male: 0.4 – 13.5 μ M female: 0.3 – 11 μ M	11 μ M	[74]
Dihydrotestosterone (DHT)	0.7 – 2.63 nM	2.6 nM	[75]
Testosterone (TEST)	male: 9.9 – 27.8 nM female: 0.2 – 2.9 nM	9.9 nM	[74]
Estradiol (E2)	male: 7.6 – 42.6 ng/L female: 8.5 – 498 ng/L	0.15 nM	[74]

Table 3. Primers used in the study

Primer name	Forward	Reverse
Parp2	GGAAGGCGAGTGCTAAATGAA	AAGGTCTTCACAGAGTCTCGATTG
Sreb1	ACATCGAAGACATGCTCCAGC	CCAGAGAAGCAGAAGAGAAGCTC
Sreb2	GCAACTTTGTAGCTCCTTCCCTG	TGGTGGGGTAGGAGAGACTTTG
Hmgcr	TGGAGATCATGTGCTGCTTC	AACTCTGGCAAATGGCTGA
Acaca	CACATGAGATCCAGCATGTCTG	TCATAAGACCACCGACGGATAG
Acyl	CACTCAGGCTTTCTCGAAGAG	TGATTAAGTGGTCTGGCTTGAC
Scd2	CCACATACTGCAAGAGATCTCTGG	CTCCAGACGTACTCCAGCTTGG
Ldlr	CGGAGTTGCAGCAGAAGACTC	TCCAGGAGTCAGGAATGCATC
Fdps	CCAAGAAAAGCAGAATTTTCATCC	GAAGACTCTCAGCATCCTGTTTC
Cyp7a1	GGAAAGTAGGTGAACCTCCTTTGG	CCGTGACATAAGACTTTGTGGTATG
Star	ATCGGGAGGGGTGGTAGTCA	TCCCCTGTTCGTAGCTGCTG
Hsd17b11	TCTTGCTGGCTTACTGCTCCA	TCCTGTTCGTCCCAAGGCAG
Srd5a1	ACGTACCACTCACCTTTCGC	TGGGAAGCCAAGGGAAGGTG
Srd5a2	GACATGCGGTTTAGCGTCCG	AAGCCACCTTGTGGGATCCTG
18S	GGGAGCCTGAGAAACGGC	GGGTCGGGAGTGGGTAATTTT
Cyclophilin	TGGAGAGCACCAAGACAGACA	TGCCGGAGTCGACAATGAT
Gapdh	CAAGGTCATCCATGACAACCTTG	GGCCATCCACAGTCTTCTGG
Insig1a	TCACAGTGACTGAGCTTCAGCA	TCATCTTCATCACACCCAGGAC
Scap	ATTTGCTCACCGTGGAGATGTT	GAAGTCATCCAGGCCACTACTAATG
Sp1	GCTACATCGACCTGACTGAGTGT	TGGTAAATAGGGTCCGCACTCAG
Sp2	TTTTGGAATGGTGTGGCGTGA	CTGCAGCGAAGAAGTAAGTCAGC

Table 4. Antibodies used in the study

* indicates validated antibodies from the <https://www.antibodypedia.com/> site.

Antibody	Company	Dilution
PARP2	Alexis, Lausen, Switzerland (ALX-210-899)*	1:1000
SREBP1	Santa Cruz, Santa Cruz, CA, USA (sc-8984)	1:1000
SREBP2	Santa Cruz, Santa Cruz, CA, USA (sc-5603)	1:1000
HMGCR	Abcam, Cambridge, UK (ab174830)	1:1000
Actin	Sigma, Saint Louis, MO, USA (A3854)	1:20000
SREBP1 (Fig. 3D)	Santa Cruz, Santa Cruz, CA, USA (2A4)	1:1000
SREBP2 (Fig. 3D)	Santa Cruz, Santa Cruz, CA, USA (1C6)	1:1000

Table 5. Human CDR ChIP-seq datasets

Cell line	GEO ID	Treatment	Pubmed ID
GM10855	GSM558630	nontr	20736230
GM10855	GSM558631	nontr	
GM10855	GSM558632	D3	
GM10855	GSM558633	D3	
GM10861	GSM558634	nontr	
GM10861	GSM558635	nontr	
GM10861	GSM558636	D3	
GM10861	GSM558637	D3	
THP1	GSM2371448	veh	28870774
THP1	GSM2371449	D3	
THP1	GSM2371450	veh	
THP1	GSM2371451	D3	
THP1	GSM2371452	veh	
THP1	GSM2371453	D3	
LX2	GSM934612	nontr	24787735
LNCaP	GSM1576449	D3	no reference

Table 6. Mouse VDR ChIP-seq data

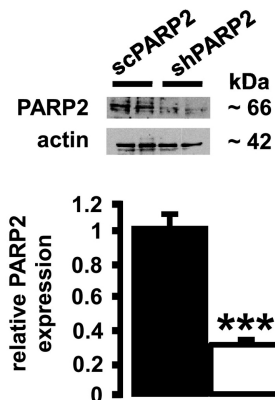
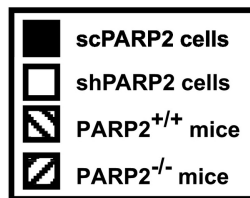
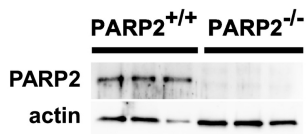
Cell line	GEO ID	Treatment	Pubmed ID
Intestine	GSM1694857	veh	26041780
Intestine	GSM1694858	veh	
Intestine	GSM1694859	veh	
Intestine	GSM1694860	D3	
Intestine	GSM1694861	D3	
Intestine	GSM1694862	D3	
MC3T3-E1	GSM1027472	veh	24891508
MC3T3-E1	GSM1027473	D3	
MSC	GSM2104114	veh	27402842
MSC	GSM2104115	veh	
MSC	GSM2104116	D3	
MSC	GSM2104117	D3	
MSC osteogenic	GSM2104150	veh	27402842
MSC osteogenic	GSM2104152	D3	
MSC adipogenic	GSM2104218	veh	
MSC adipogenic	GSM2104220	D3	

Highlights

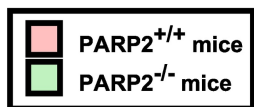
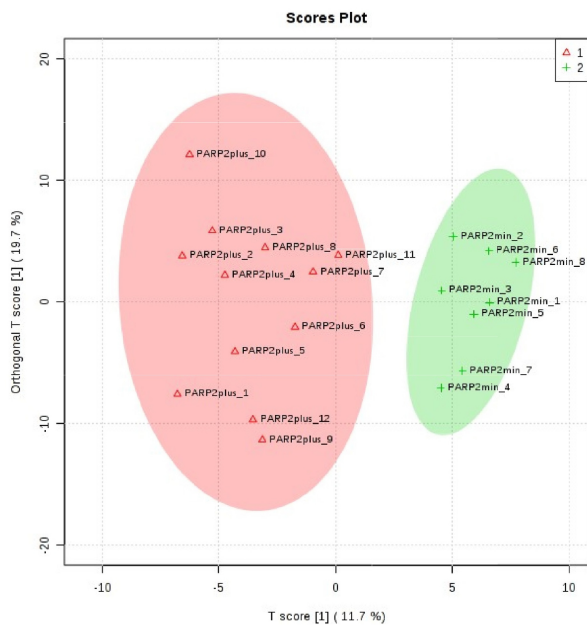
1. The genetic deletion of poly(ADP-ribose)-2 (PARP2) induces characteristic changes in the lipidome.
2. In PARP2 knockout mice SREBP1 and SREBP2 is overexpressed in skeletal muscle leading to higher muscular cholesterol biosynthesis.
3. Higher muscular cholesterol is shunted towards muscular dihydrotestosterone synthesis, but is not translated into systemic increases in dihydrotestosterone levels.
4. The muscles from PARP2 knockout mice are stronger as compared to the ones derived from wild type littermates.
5. The expression of PARP2 is regulated by cholesterol derivatives.

ACCEPTED MANUSCRIPT

A



B

PARP2 $^{+/+}$ / PARP2 $^{-/-}$ mice

sc/shPARP2 C2C12 cells

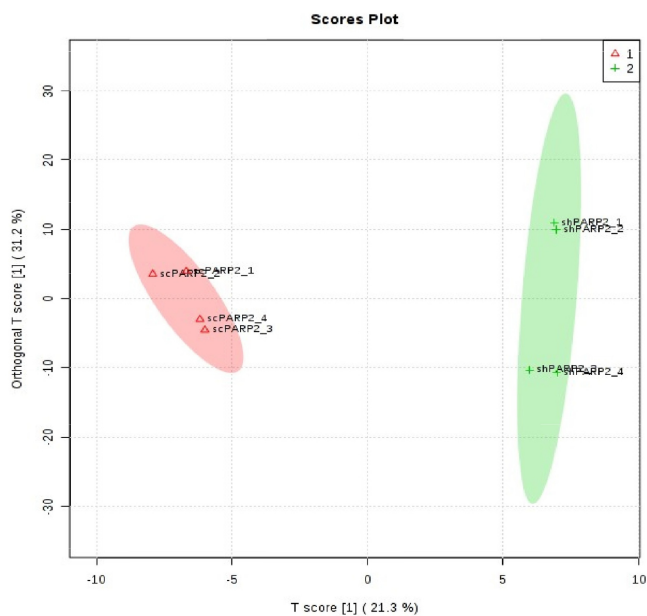


Figure 1

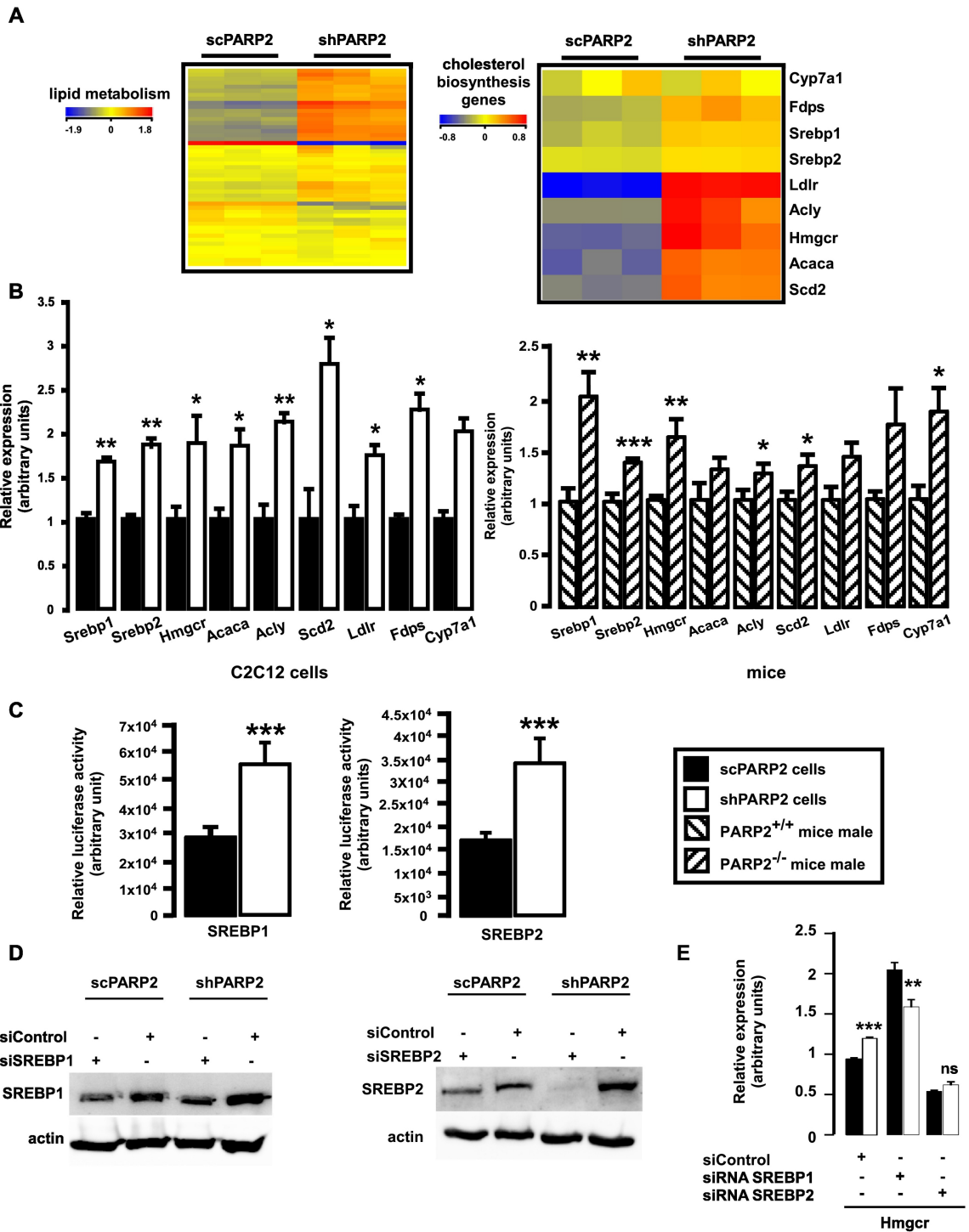


Figure 2

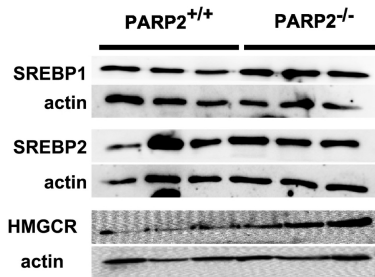
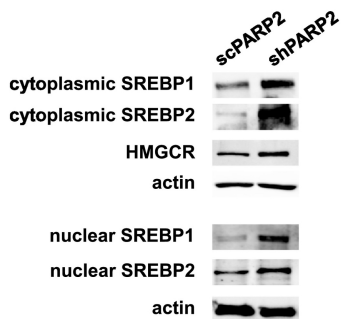
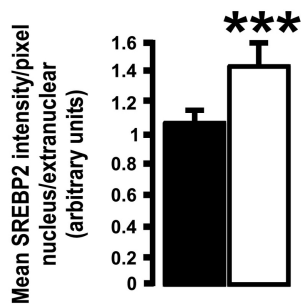
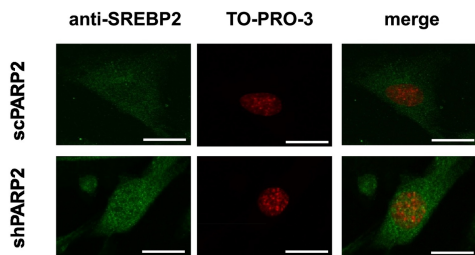
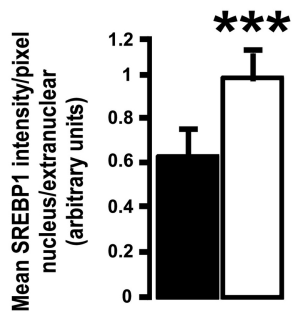
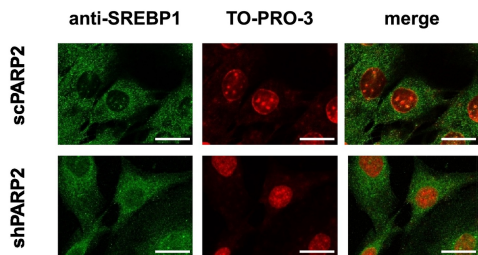
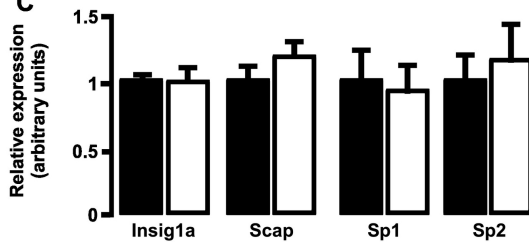
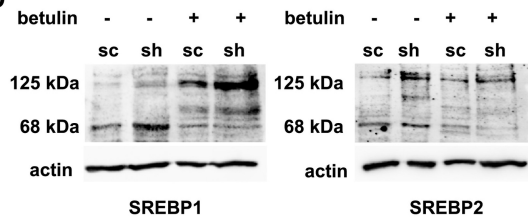
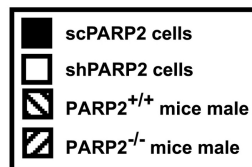
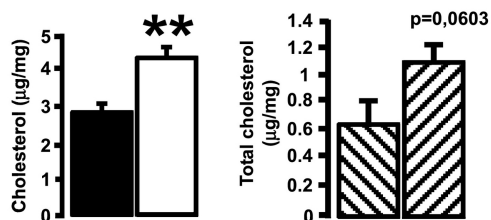
A**B****C****D****E**

Figure 3

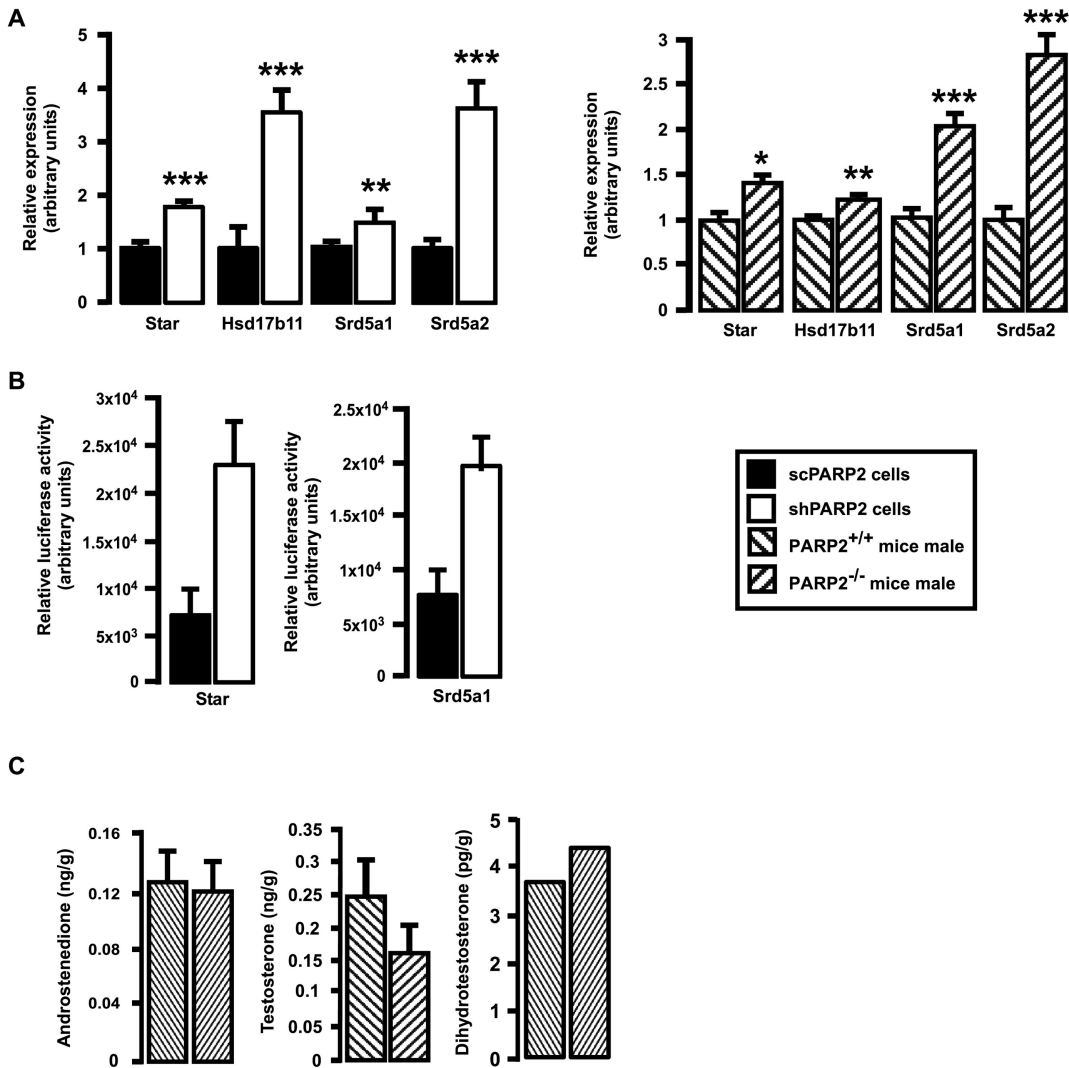


Figure 4

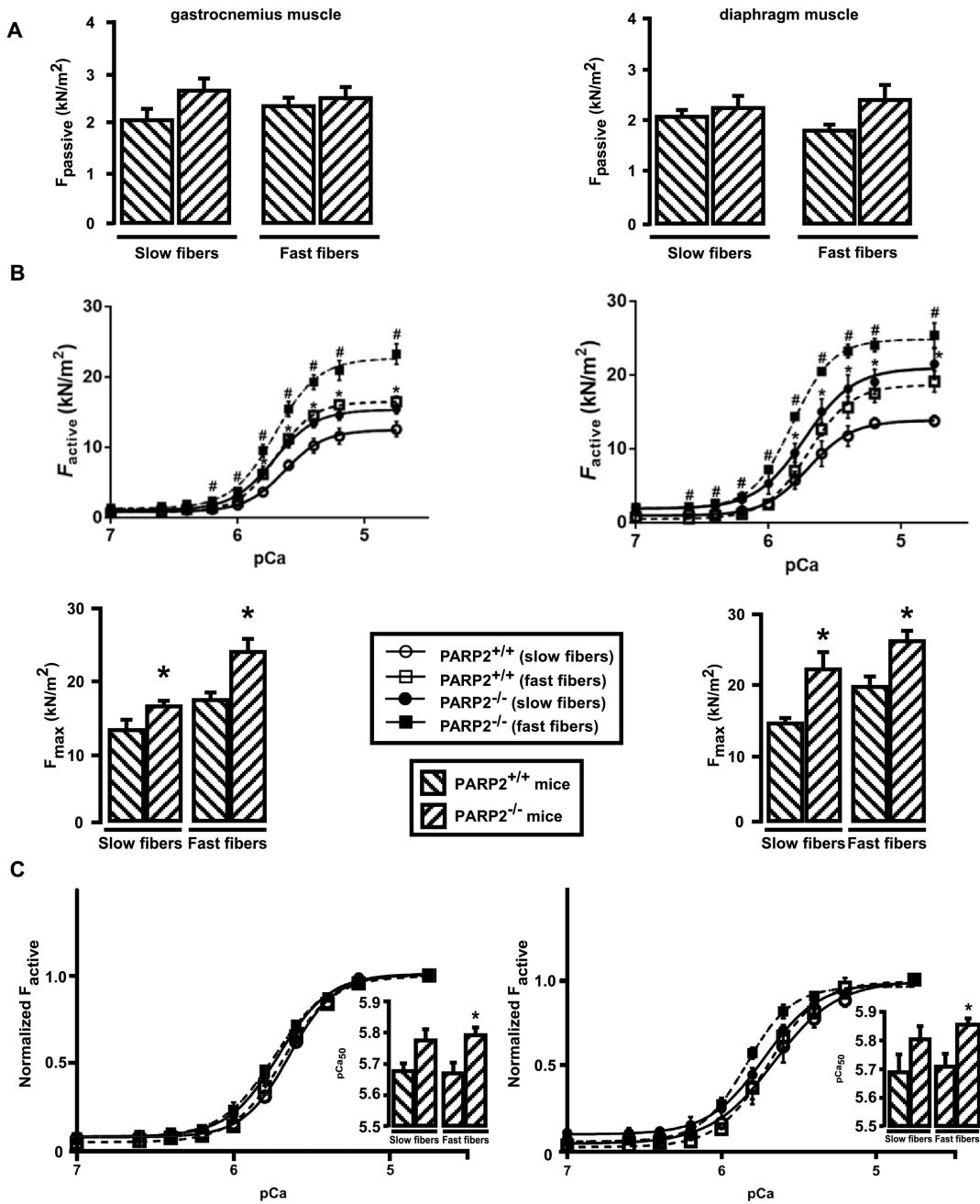
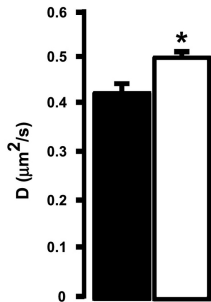
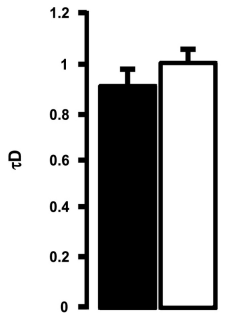


Figure 5

A

Diffusion constant of bodipy-FL-SM

B

τD of bodipy-FL-SM

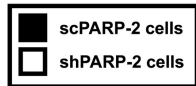
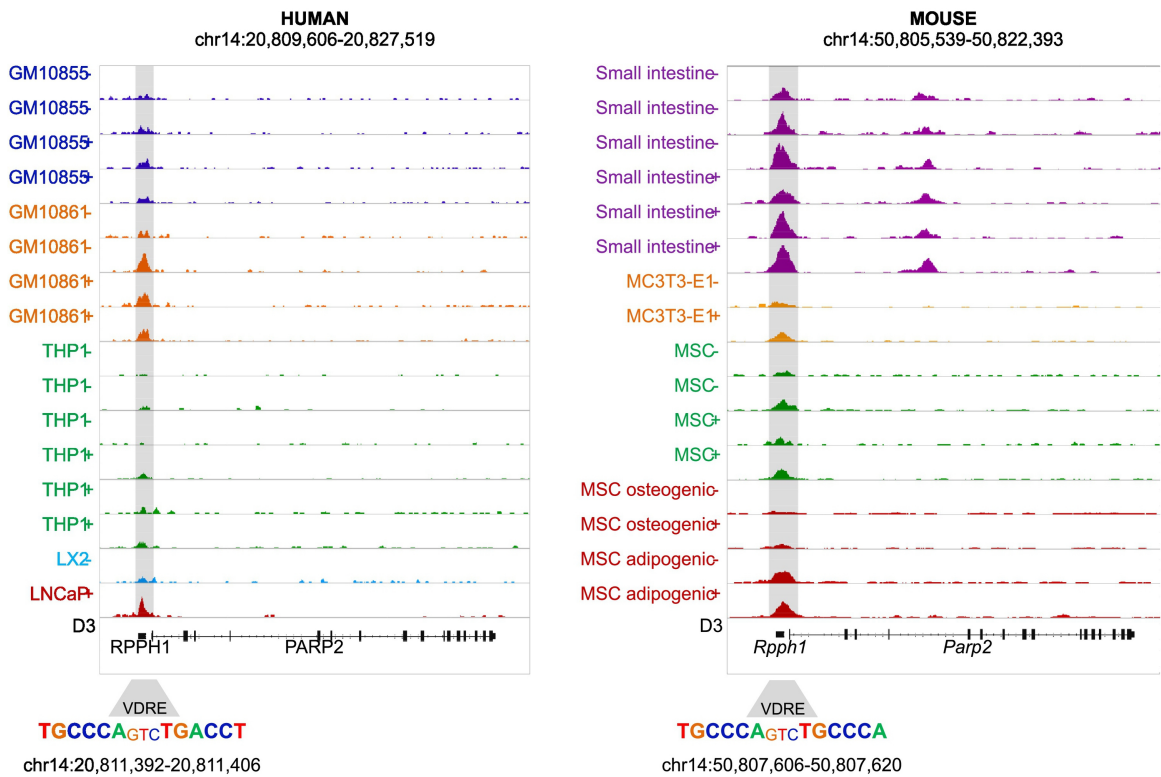


Figure 6

A



B

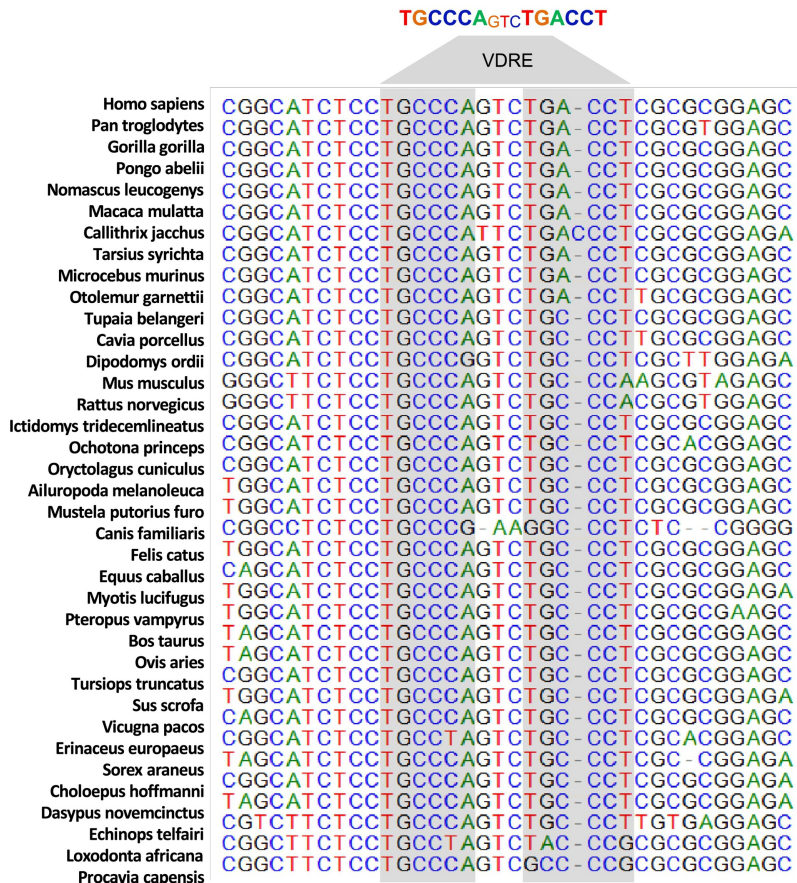


Figure 7

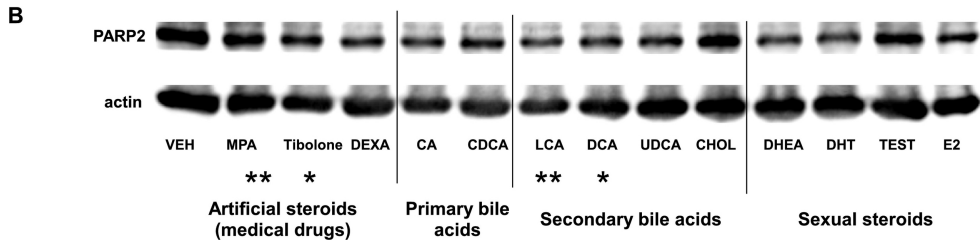
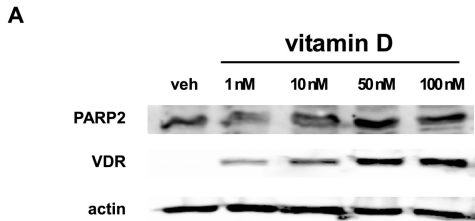


Figure 8